Deep sourced fluids for peridotite carbonation in the shallow mantle wedge of a fossil subduction zone: Sr and C isotope profiles of OmanDP Hole BT1B

Juan Carlos de Obeso[1,2], Peter B. Kelemen[2], James M. Leong[2], Manuel D. Menzel[3], Craig E. Manning[4], Marguerite Godard[5], Yue Cai[2], Louise Bolge[2] and Oman Drilling Project Phase 1 Science Party

[1] Department of Geosciences, University of Calgary, Calgary, Canada
[2] Lamont Doherty Earth Observatory Columbia University, Palisades, NY, USA.
[3] Institute of Tectonics and Geodynamics, RWTH Aachen University, Aachen, Germany.
[4] Dept. of Earth & Space Sciences, University of California, Los Angeles, CA, USA.
[5] Géosciences Montpellier, Université de Montpellier, Montpellier, France.

Corresponding author: Juan Carlos de Obeso (juancarlos.deobeso@ucalgary.ca)

Key Points:

- Strontium and Carbon were added to the peridotites during alteration of mantle peridotite with carbonated fluid derived from decarbonation reaction.

Abstract

Completely carbonated peridotites represent a window to study reactions of carbon-rich fluids with mantle rocks. Here we present details on the carbonation history of listvenites close to the basal thrust in the Samail ophiolite. We use samples from Oman Drilling Project Hole BT1B, which provides a continuous record of lithologic transitions, as well as outcrop samples from listvenites, metasediments and metamafics below the basal thrust of the ophiolite. $^{87}Sr/^{86}Sr$ of listvenites and serpentinites, ranging from 0.7090 to 0.7145, are significantly more radiogenic than mantle values, Cretaceous seawater, and other peridotite hosted carbonates in Oman. The Hawasina metasediments that underlie the ophiolite, on the other hand, show higher $^{87}Sr/^{86}Sr$ values of up to 0.7241. $\delta^{13}C$ values of total carbon in the listvenites and serpentinites range from -10.6‰ to 1.92‰. We also identified a small organic carbon component with $\delta^{13}C$ as low as -27‰. Based on these results, we propose that during subduction at temperatures above 500°C, carbon-rich fluids derived from decarbonation of the underlying sediments migrated up dip and generated the radiogenic $^{87}Sr/^{86}Sr$ signature and the fractionated $\delta^{13}C$ values of the serpentinites and listvenites in core BT1B.

Plain Language Summary

Samples from Oman Drilling Project Hole BT1B provide a record of interactions of fluids rich in carbon dioxide with mantle rocks. This interactions lead to the formation of listvenites, rocks composed mainly by magnesite and quartz. Here we describe the formation of listvenites in the Oman ophiolite using Strontium and Carbon isotopes to characterize the source and nature of the fluid that pervasively transform the mantle rocks that now store vast amounts of carbon dioxide.

1 Introduction

Hydration and carbonation of ultramafic rocks are important processes in the carbon and water cycle of our planet (Alt et al., 2013; Fruh-Green et al., 2004). These alteration reactions are sinks of water and carbon where peridotites are exposed on the seafloor forming alteration minerals like serpentine and carbonates (Alt et al., 2013; Klein et al., 2020; Macdonald & Fyfe, 1985; Paulick et al., 2006) which are carried back into the mantle in convergent margins. Fluids derived from the subducted slab can migrate and interact with the mantle wedge in subduction zones, so that the "leading edge of the mantle wedge" aka the "cold nose", can be partially hydrated and carbonated (Blakely et al., 2005; Hyndman & Peacock, 2003; Peter B. Kelemen & Manning, 2015). This is usually inferred from seismic data (e.g. DeShon and Schwartz, 2004; Kamiya and Kobayashi, 2000; Tibi et al., 2008; Tsuji et al., 2008). Understanding the interaction of carbon-bearing hydrous fluids with peridotites is important to supplement and constrain geophysical observations.

Fully carbonated peridotites, also known as listvenites, provide a window into the alteration processes that occur in the "cold nose" of the mantle wedge above subduction zones, where mantle peridotite reacts with hydrous and carbonated fluids likely derived from the subducting slab at moderate temperatures and pressures (Beinlich et al., 2012; Boskabadi et al., 2017, 2020; Falk & Kelemen, 2015; Manuel D. Menzel et al., 2018). Formation of listvenites appears to be restricted to particular conditions requiring high carbon concentrations in the fluid

(Falk & Kelemen, 2015; Hansen et al., 2005; Peter B. Kelemen et al., 2021; Manuel D. Menzel et al., 2018). For example, complete carbonation of peridotites to form listvenites is not observed near the surface in ophiolites (e.g. Clark and Fontes, 1990; de Obeso and Kelemen, 2020, 2018; Garcia del Real et al., 2016; Kelemen and Matter, 2008; Noël et al., 2018; Quesnel et al., 2016; Schwarzenbach et al., 2016). It is also not observed near the seafloor, where serpentinization and formation of carbonate veins are common (e.g Bach et al., 2011; Delacour et al., 2008; Schwarzenbach et al., 2013). Fluid sources for complete carbonation have been associated with subduction in different listvenite localities. Menzel at al. (2018) attributed carbonation of harzburgite in the Advocate ophiolite (Canada) to fluxing by slab-derived, CO_2-rich fluids. Isotopic data ($\delta^{13}C$, $\delta^{18}O$ and $^{87}Sr/^{86}Sr$) of listvenites in the Late Cretaceous ophiolites of eastern Iran point to carbon-bearing fluids derived from subducted sedimentary units as the source of carbon (Boskabadi et al., 2020).

In Oman, listvenites occur along the basal thrust of the ophiolite (Nasir et al., 2007; Wilde et al., 2002). Previous studies have investigated their formation conditions and the nature of the carbonation fluids without reaching conclusive answers on the source of the fluids (Beinlich et al., 2020; Falk & Kelemen, 2015; Nasir et al., 2007; Stanger, 1985). In this paper, we present $^{87}Sr/^{86}Sr$ and $\delta^{13}C$ data on samples from Oman Drilling Project Hole BT1B and the underlying sediments of the Hawasina Formation. We show that devolatization of the subducting sediments similar to the Hawasina Formation likely generated the carbonation fluids which reacted with the mantle wedge in this fossil subduction zone to form listvenites. These processes probably operate in subduction zones worldwide, where fluids migrate updip along the slab mantle interface, and then react with hanging wall peridotites. Our results have implications for the global carbon cycle, as significant amounts of carbon could be stored in the mantle during mantle wedge carbonation.

2 Geological setting

2.1 The Samail ophiolite

The Samail ophiolite, along the northeast coast of Oman and the United Arab Emirates (UAE), is the best-exposed block of oceanic crust and its underlying mantle in the world. It was thrust over adjacent oceanic lithosphere soon after magmatic formation, and then onto the margin of the Arabian subcontinent in the late Cretaceous. The mantle section of the ophiolite is mainly composed of highly depleted, residual mantle peridotites (mostly harzburgites, e.g. (Godard et al., 2000; Hanghøj et al., 2010; Monnier et al., 2006), together with 5 to 15% dunite (Braun, 2004; Braun & Kelemen, 2002; Collier, 2012). Near the basal thrust, interlayered dunites and refertilized harzburgites comprise the distinctive “Banded Unit” (Khedr et al., 2014). The peridotites are pervasively serpentinized, with serpentine (± brucite) making up ~ 30-100 wt% of “fresh” rock (Godard et al., 2000; Hanghøj et al., 2010; Monnier et al., 2006) and/or completely carbonated to form listvenites (Falk & Kelemen, 2015; Nasir et al., 2007; Stanger, 1985; Wilde et al., 2002). The listvenites only occur within a few km of the basal thrust of the ophiolite, and

within the tectonic melanges with a serpentine matrix just below the base of the ophiolite (Nasir et al., 2007; Stanger, 1985).

2.2 Lithologies below the Samail ophiolite nappe

Beneath the mantle section of the Samail ophiolite is a locally preserved "metamorphic sole". This sole is exposed discontinuously along the basal thrust, juxtaposed with the overlying Banded Unit at the base of the Samail mantle section. It records peak metamorphic temperatures of 700-900°C and imprecise peak pressures of 0.8 to 1.4 GPa (Cowan et al., 2014; Hacker & Mosenfelder, 1996; M. P. Searle & Malpas, 1980; Michael P. Searle & Cox, 2002; Soret et al., 2017). A lower temperature unit (~450-550°C) with similar peak pressures (0.8 to 1.2 GPa) has also been identified from the metamorphic section of Oman DP Hole BT1B (Kotowski et al., 2021). The base of the sole is in fault contact with low grade allochthonous sediments of the Hawasina formation, which is composed of pelagic clastic units interlayered with limestones (Bechennec et al., 1990; Béchennec et al., 1988) deposited from the late Permian to the Cretaceous. The Hawasina sedimentary units were thrusted over autochthonous Mesozoic to Proterozoic platform sediments of the Arabian continental margin, forming nappes between the autochton and the ophiolite.

2.3 *OmanDP Hole BT1B and Oman Listvenites*

Hole BT1B was drilled in March 2017 in Wadi Mansah (23.364374°N, 58.182693°E), which yielded a total length of 300.1 m with 100% recovery (Kelemen et al., 2020). The upper 6 meters are composed of alluvial gravels followed by an ultramafic sequence comprised of listvenites (carbonated peridotites) interlayered with two serpentinite bands (80-100 m depth and 181 to 186 m depth). A thick (0.42 m) layer of grey-green fault gouge at 196.6 m–197.1 m depth separates the ultramafic units from the metamorphic sole composed of fine-grained metasediments and metabasalts (Kelemen et al., 2021; Kelemen et al., 2020). To the first order, alteration of peridotite to form serpentinite and listvenite in Hole BT1B was nearly isochemical except for the addition of H_2O and CO_2. Average bulk rock Mg/Si, Fe/Si, Al/Si, Fe/Mg, and Cr/Al ratios in serpentinite and listvenite are close to the average composition of the Samail peridotite (Kelemen et al. 2020, Kelemen et al. 2021) and similar to the composition of previously studied listvenites from the outcrops extending north and northeast from the drill site (Falk & Kelemen, 2015). The core provides a unique record of the interaction between peridotite in the leading edge of the mantle wedge and hydrous, CO_2-rich fluids derived from subducted lithologies. For an expanded version of the geology of Oman DP Hole BT1B and MoD mountain we refer the reader to the Proceedings of the Oman Drilling Project (Kelemen et al., 2020) and Kelemen et al. (2021) in this Special Issue.

3 Materials and Methods

Samples analyzed for this study comprise a suite of drill core samples from OmanDP Hole BT1B and hand samples of the Hawasina formation. Drill core samples encompass all the identified lithologies from Hole BT1B. Major element compositions for Hole BT1B samples were reported in the *Proceedings of the Oman Drilling Project* (Kelemen et al 2020) with the exception of samples in the 181-186m depth interval which are reported by Godard et al. Trace element compositions of Hole BT1B samples can be found in Godard et al. Trace element

compositions and loss on ignition for Hawasina formation outcrop samples were analyzed at Lamont Doherty Earth Observatory (LDEO). Rb and Sr concentrations were analyzed using a VG PlasmaQuad ExCell quadrupole ICP-MS following HNO_3-HF digestion. Major element compositions of the Hawasina samples are available in supplementary table 1. Additional Sr isotopes were measured on samples from outcrops northeast of Hole BT1B (Falk & Kelemen 2015).

For Sr isotope analysis, bulk rock powder was fully digested in a HNO_3-HF mixture overnight and redissolved in 3N HNO_3 prior to column chemistry using the Eichrom® Sr resin. Purified Sr were analyzed for isotopic compositions interspersed with US National Institute of Standards and Technology (NIST) SRM 987 on a Thermo Scientific Neptune multi-collector ICP-MS at LDEO. In-run mass fractionations were normalized to $^{86}Sr/^{88}Sr=0.1194$. Unknowns were normalized to SRM 987 $^{87}Sr/^{86}Sr$ value of 0.701248. International standards BHVO-2 yielded $^{87}Sr/^{86}Sr$ value of 0.703509±41 (2σ, n = 3) and BCR-2 yielded 0.705046±34 (2σ, n = 3), which agree with published values from Weis et al. (2006).

Total Carbon (TC) was measured from the same bulk rock powder splits as for Strontium isotopes. Total Organic Carbon (TOC, or reduced carbon) was measured from the residual rock powder after the removal of Inorganic Carbon (carbonate carbon) through reaction with dilute (3 N) HCl for at least 3 days, followed by washing with Millipore® water. Concentrations and $\delta^{13}C$ ratios of total carbon (TC) and total organic carbon (TOC), were determined using a Costech element analyzer coupled with a Thermo Scientific Delta V plus mass spectrometer at LDEO. Sample runs were calibrated using Acetanilide for carbon contents ($R^2=0.9998$). For $\delta^{13}C$ we used USGS40 ($\delta^{13}C$ =-26.77±0.16‰ V-PDB, n=4), USGS41 ($\delta^{13}C$ =37.63±0.12‰ V-PDB, n=4) and USGS24 ($\delta^{13}C$ =-16.04±0.13‰ V-PDB, n=4). All measured values of $\delta^{13}C$ standards agree

with accepted values reported by the United States Geological Survey (USGS). Inorganic carbon contents and $\delta^{13}C$ of TIC were estimated by mass balance between TC and TOC.

3 Results

Depth profiles of $^{87}Sr/^{86}Sr$, Sr and Rb concentrations, carbon concentrations, Total Carbon and Total carbon $\delta^{13}C$ are shown in Figure 1 and Table 1 and 2. The Hawasina sediments are plotted with respect to map distance to the closest metamorphic sole/ultramafic contact.

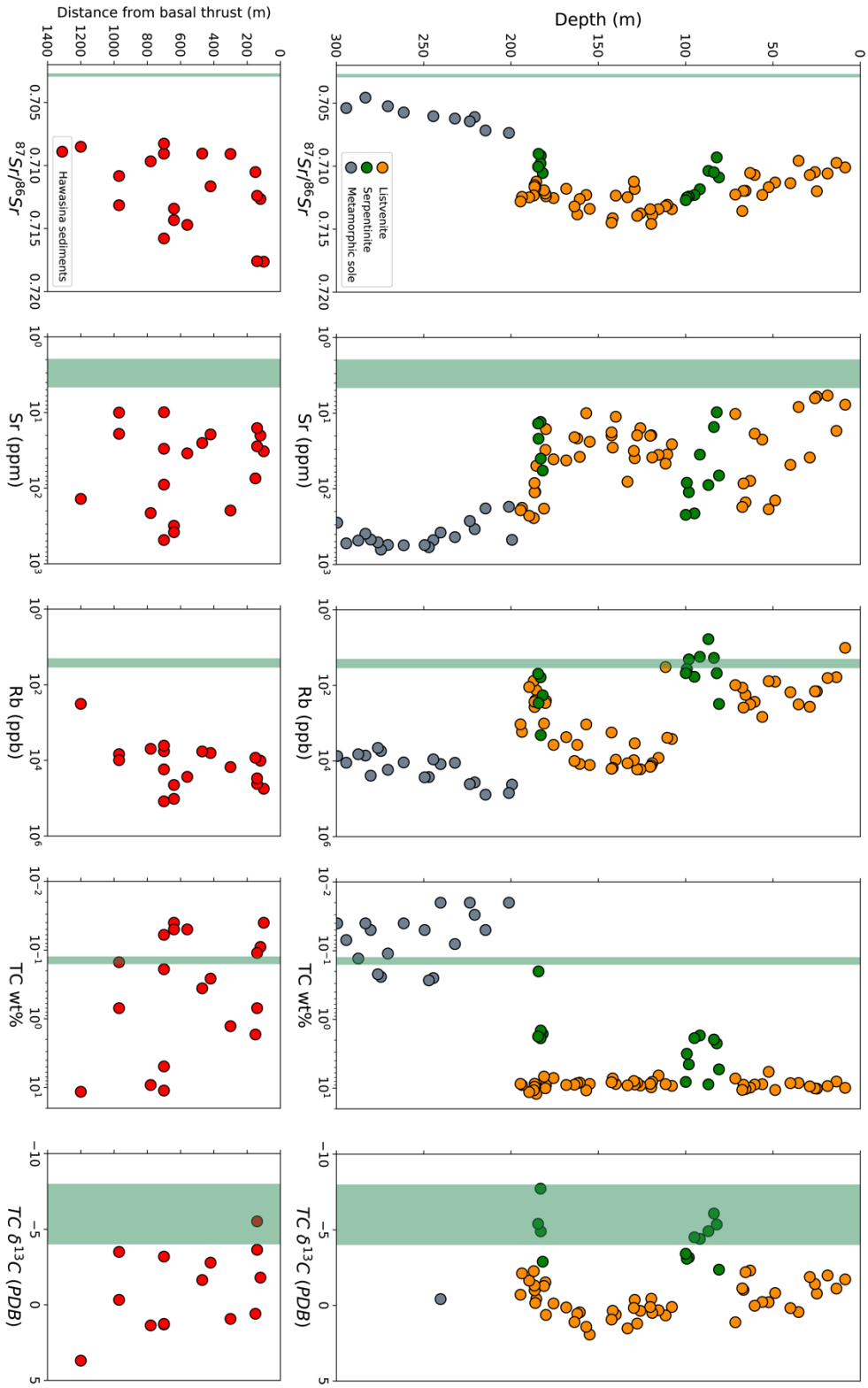
Depth (m)
Distance from basal thrust (m)
Listvenite
Serpentinite
Metamorphic sole
Hawasina sediments
$^{87}Sr/^{86}Sr$
Sr (ppm)
Rb (ppb)
TC wt%
TC $\delta^{13}C$ (PDB)

170

171

172 **Figure 1.** Depth profiles of OmanDP Hole BT1B and distance from basal thrust for Hawasina
173 sediments. From left to right $^{87}Sr/^{86}Sr$ (measured), Sr concentrations, Rb concentrations, total
174 carbon (TC) concentration, total carbon $\delta^{13}C$. Green bands for reference from left to right are
175 average MORB $^{87}Sr/^{86}Sr$ (measured) (Gale et al., 2013; Hofmann, 2013), Oman harzburgite
176 average Sr (ppm) and Rb (ppb) (Godard et al., 2000; Hanghøj et al., 2010; Monnier et al., 2006),
177 Oman harzburgite average total carbon (TC) (Peter B. Kelemen & Manning, 2015), average
178 mantle $\delta^{13}C$ (Deines, 2002). The distance from the basal thrust for the Hawasina sediments
179 (bottom panels) is measured as the horizontal distance to the closest mapped metamorphic
180 sole/ultramafic contact.

181

Sample	Depth CCD (m)	Lithology	87Sr/86Sr	2SE total error	Rb (ppb)	Sr (ppb)	TC (wt%)	TC d13C (‰PDB)	OC (wt%)	TOC (d13C ‰PDB)
C5704B_7Z4_14-19	8.64	listvenite	0.7101029	0.000023	10	7733	9.9	-1.72	NA	NA
C5704B_9Z3_23-28	13.67	listvenite	0.7097414	0.000022	61	17156	8.01	-1.12	NA	NA
C5704B_12Z1_84-89	18.72	listvenite	0.7105864	0.000023	64	5844	9.32	-1.98	NA	NA
C5704B_14Z2_25-30	24.86	listvenite	0.7119908	0.000023	144	6042	10.16	-0.79	0.04	-14.58
C5704B_14Z3_71-76	25.93	listvenite	0.710479	0.000019	143	6351	10.08	-1.42	1.48	-2.88
C5704B_16Z3_7-12	28.9	listvenite	0.7107064	0.000021	368	38660	9.42	-1.88	NA	NA
C5704B_18Z3_25-31	35.34	listvenite	0.7095716	0.000023	319	8284	8.42	0.44	1.49	NA
C5704B_20Z1_78-83	40.01	listvenite	0.7113509	0.000022	152	48281	8.46	0.18	NA	NA
C5704B_23Z1_37-42	48.75	listvenite	0.711299	0.000019	80	142571	10.63	-0.82	0.07	-19.07
C5704B_25Z2_55-60	52.45	listvenite	0.7116712	0.000020	78	186366	5.78	-0.21	0.02	-17.36
C5704B_26Z2_77-82	56.11	listvenite	0.7122875	0.000019	682	22385	8.76	-0.23	NA	NA
C5704B_28Z1_69-74	60.47	listvenite	0.7106974	0.000020	272	18688	8.86	0.02	0.09	-13.68
C5704B_30Z2_53-58	63.07	listvenite	0.7105413	0.000021	318	78656	9.82	-2.31	NA	NA
C5704B_31Z3_31-37	65.71	listvenite	0.7119567	0.000019	178	151322	10.3	-2.20	0.22	-6.87
C5704B_32Z1_19-24	66.87	listvenite	0.7119635	0.000020	386	85105	8.92	-1.03	0.88	-4.52
C5704B_32Z2_7-12	67.55	listvenite	0.7135589	0.000019	115	174106	10.61	-1.13	2.43	NA
C5704B_35Z1_6-11	71.54	listvenite	0.7122553	0.000022	98	10237	7.23	1.11	0.89	NA
C5704B_38Z3_86-91	80.9	serpentinite	0.7108931	0.000022	310	66812	5.33	-2.37	0.09	-10.07
C5704B_39Z1_25-30	82.18	serpentinite	0.709307	0.000022	48	9733	2.23	-5.35	0.10	-13.67
C5704B_39Z3_13-8	83.81	serpentinite	0.7104894	0.000021	19	15271	1.96	-6.08	0.03	-22.04
C5704B_40Z3_3-8	86.98	serpentinite	0.710374	0.000019	6	89171	8.81	-4.91	0.06	-24.23
C5704B_42Z2_26-31	91.85	serpentinite	0.7118308	0.000021	18	35313	1.71	-4.40	0.07	NA
C5704B_43Z2_3-8	94.96	serpentinite	0.712288	0.000019	59	211715	1.87	-4.51	0.07	NA
C5704B_44Z2_29-34	98.17	serpentinite	0.7124092	0.000019	21	110987	4.52	-3.17	0.04	-15.24

C5704B_44Z3_57-62	99.31	serpentinite	0.7124888	0.000023	37	83218	3.16	-3.08	0.06	-26.45
C5704B_44Z4_50-55	99.94	serpentinite	0.7127018	0.000020	47	221049	8.11	-3.42	0.29	-4.90
C5704B_47Z3_18-23	107.88	listvenite	0.7134127	0.000020	2612	25806	9.26	0.10	0.05	-23.97
C5704B_48Z2_26-31	110.52	listvenite	0.7130681	0.000022	2429	35139	NA	NA	0.02	-25.40
C5704B_48Z3_90-95	111.5	listvenite	0.7131781	0.000023	33	46533	8.74	0.66	NA	NA
C5704B_50Z4_65-70	115.53	listvenite	0.7134198	0.000023	8287	35574	6.55	0.32	NA	NA
C5704B_52Z1_60-65	119.13	listvenite	0.7138657	0.000019	11406	38542	8.1	0.49	0.44	-5.64
C5704B_52Z3_0-5	119.67	listvenite	0.7145867	0.000022	13213	19572	9.72	-0.44	NA	NA
C5704B_52Z3_61-66	120.28	listvenite	0.7134184	0.000019	14220	19930	8.64	0.10	NA	NA
C5704B_54Z2_47-52	125.92	listvenite	0.7137525	0.000022	16514	15830	9.15	0.36	NA	NA
C5704B_55Z1_8-13	127.76	listvenite	0.7139473	0.000022	16596	19674	8.37	1.20	0.07	NA
C5704B_55Z2_59-64	129.16	listvenite	0.7118074	0.000020	3417	39477	8.84	-0.37	0.11	-4.23
C5704B_55Z3_15-20	129.65	listvenite	0.7112276	0.000022	9522	31563	7.87	0.16	NA	NA
C5704B_56Z4_11-16	133.29	listvenite	0.7124671	0.000022	11464	80713	9.11	1.52	NA	NA
C5704B_60Z1_12-17	140	listvenite	0.7123404	0.000022	9275	11158	8.69	0.61	NA	NA
C5704B_60Z3_40-45	141.79	listvenite	0.7141358	0.000019	15152	28514	7.22	0.35	0.31	0.74
C5704B_60Z4_24-29H	142.43	listvenite	0.7144926	0.000020	16037	19667	8.21	0.93	NA	NA
C5704B_64Z4_18-23	154.95	listvenite	0.7133899	0.000020	12775	23908	8.68	1.93	NA	NA
C5704B_65Z3_33-38	156.91	listvenite	0.7122888	0.000020	1079	10005	10.76	1.41	0.10	-16.35
C5704B_66Z3_66-71	160.62	listvenite	0.7126074	0.000022	11964	37852	8.31	0.45	0.06	-24.15
C5704B_67Z2_26-31	162.03	listvenite	0.7138291	0.000022	3747	21596	8.48	0.55	NA	NA
C5704B_67Z4_39-44	163.67	listvenite	0.7131952	0.000019	10001	20778	8.89	1.10	0.04	-10.87
C5704B_69Z2_55-63	168.38	listvenite	0.7117951	0.000023	2341	42165	8.98	0.13	NA	NA
C5704B_71Z4_0-8	175.63	listvenite	0.7125344	0.000018	3745	40763	7.12	-0.13	0.05	-16.71
73-1-71.0-75.0cm	180.01	listvenite	0.7123924	0.000022	254	16269	9.1	0.63	0.24	-4.63
C5704B_73Z2_0-5	180.3	listvenite	0.71218	0.000020	292	30626	10.04	-1.53	0.21	-8.61
73-3-8.0-13.0cm	181.1	listvenite	0.7119166	0.000022	1021	182886	6.79	-1.29	0.02	-14.10
73-4-11.0-16.0cm	181.85	serpentinite	0.7105479	0.000022	182	57427	1.62	-2.89	0.04	-16.58
C5704B_74Z1_56-64	182.95	serpentinite	0.7091689	0.000023	2073	39906	1.45	-4.90	0.05	-27.04
74-2-0.0-5.0cm	183.07	serpentinite	0.7097785	0.000017	61	13067	1.88	-7.72	0.07	-10.96
74-3-42.0-47.0cm	184.24	serpentinite	0.7090228	0.000019	294	21788	0.2	-10.62	0.04	-24.59
74-3-67.0-73.0cm	184.49	serpentinite	0.7100467	0.000023	49	13717	1.77	-5.40	0.24	-9.94
75-1-12.0-16.0cm	185.52	listvenite	0.7112295	0.000022	134	49603	12.12	-0.43	0.10	-17.53
75-1-70.0-75.0cm	186.1	listvenite	0.7117597	0.000020	247	110258	9.7	-0.16	0.16	NA

75-2-27.0-32.0cm	186.46	listvenite	0.7115092	0.000022	373	111620	8.61	-1.00	0.07	NA
C5704B_75Z2_31-40	186.54	listvenite	0.7116533	0.000021	272	84029	9.54	-1.32	0.11	-11.87
75-2-76.0-82.0cm	186.95	listvenite	0.7123277	0.000019	76	244293	10.73	-2.27	0.69	NA
C5704B_76Z2_38-42	189.58	listvenite	0.7124782	0.000019	111	227322	11.43	-1.64	0.33	-12.42
C5704B_77Z3_40-48	193.71	listvenite	0.7124411	0.000019	1696	178429	8.98	-2.12	0.26	-5.61
C5704B_77Z4_43-48	194.57	listvenite	0.7127999	0.000020	1072	192155	8.66	-0.71	0.17	-9.16
C5704B_82Z1_50-55	201.18	Metamorphic	0.7073636	0.000020	70152	173001	0.02	NA	NA	NA
C5704B_88Z2_76-82	214.59	Metamorphic	0.7071713	0.000018	77502	182069	0.05	NA	NA	NA
C5704B_90Z3_8-13	220.79	Metamorphic	0.7061036	0.000019	36796	341585	0.03	NA	NA	NA
C5704B_92Z3_0-8	223.58	Metamorphic	0.7064436	0.000020	40839	266694	0.02	NA	NA	NA
C5704B_96Z2_0-8	232.1	Metamorphic	0.7062253	0.000019	11143	436010	NA	NA	0.09	-19.25
C5704B_99Z1_0-5	240.33	Metamorphic	NA	NA	12063	378913	0.02	-0.42	NA	NA
C5704B_100Z2_13-21	244.47	Metamorphic	0.7060383	0.000018	9065	477887	0.25	NA	NA	NA
C5704B_105Z4 31-36	261.44	Metamorphic	0.705739	0.000019	10901	558612	0.04	NA	NA	NA
C5704B_109Z4 24-32	270.5	Metamorphic	0.7052469	0.000020	17054	553129	0.11	NA	NA	NA
C5704B_116Z1_31-39	283.35	Metamorphic	0.7045642	0.000019	7182	392644	0.04	NA	NA	NA
C5704B_124Z1 53-61	294.32	Metamorphic	0.7053928	0.000018	11092	527027	0.07	NA	NA	NA

Table 1. OmanDP Hole BT1B Strontium and Carbon concentrations and isotope rations

Sample	Latitude	Longitude	Elevation (m)	Distance from Basal thrust (m)	Sr (ppm)	Rb (ppm)	87Sr/86Sr	2SE total error	C (wt%)	d13C (‰ PDB)
OM20-01	23.3727	58.18973	556	NA	360.92	3.6	0.7093033	0.000008	0.99	-0.61
OM20-03	23.35872	58.23122	364	420	19.47	6.38	0.7116514	0.00001	0.26	-2.79
OM20-05	23.37326	58.51663	468	470	25.23	5.8	0.7090506	0.000007	0.36	-1.64
OM20-06	23.3763	58.21493	493	640	314.26	44.7	0.7134211	0.000007	0.04	NA
OM20-07	23.37628	58.21508	488	640	382.46	103.96	0.7143305	0.000007	0.05	NA
OM20-08	23.35756	58.21843	418	120	20.15	10.2	0.7126578	0.000007	0.09	-1.8
OM20-09	23.35744	58.21829	432	100	32.54	56.28	0.7176305	0.000006	0.04	NA
OM20-11	23.35789	58.21856	454	140	16.06	41.9	0.7175916	0.00001	0.11	-5.52
OM20-12	23.38609	58.14561	262	780	213.39	4.94	0.7096678	0.000009	9.18	1.36
OM20-13	23.39792	58.18225	278	150	74.29	8.52	0.7105193	0.000006	1.69	0.59
OM20-14	23.40735	58.15496	269	700	9.9	17.3	0.7157845	0.000008	0.19	-3.19
OM20-15	23.40758	58.1547	265	700	89.69	5.73	0.7090595	0.000009	4.93	1.3

OM20-16	23.39377	58.17862	302	560	34.61	27.25	0.7147076	0.000006	0.05	NA
OM20-17	23.40754	58.1546	273	700	30.13	121.1	0.7241322	0.000009	0.06	NA
OM20-10	23.35786	58.21854	458	140	27.97	29.92	0.712403	0.000007	0.7	-3.64
OM20-18	23.40763	58.15468	275	700	484.97	4.07	0.7082638	0.000009	11.06	1.26
OM20-19	23.39655	58.04998	310	300	197.35	15.03	0.7090828	0.000007	1.28	0.93
OM20-42	23.414996	58.161405	253	1200	138.71	0.32	0.7085112	0.00001	11.53	3.69
OM20-04a	23.36214	58.23478	384	970	19.13	6.84	0.7108331	0.000009	0.7	-0.33
OM20-04B	23.36214	58.23478	384	970	10.01	9.86	0.71315	0.000008	0.15	-3.5

Table 2. Hawasina metasediments Strontium and Carbon concentrations and isotope rations

3.1 Strontium Isotopes

Measured $^{87}Sr/^{86}Sr$ values in Oman DP Hole BT1B lithologies show clear differences between (a) the metamorphic sole and (b) the listvenites and serpentinites. The listvenites and serpentinites vary from a minimum value of 0.709 in the upper serpentinite band to a maximum of 0.715 in some listvenites. $^{87}Sr/^{86}Sr$ values in the listvenites increase with depth from the surface to 150 m while the serpentinite band between 80-100 m have lower values. Below 150 m, $^{87}Sr/^{86}Sr$ values are relatively constant with increasing depth, until the second serpentine band at 181-186 m. Below the basal thrust, $^{87}Sr/^{86}Sr$ values are significantly lower in the metamorphic sole from 0.704 to 0.706, followed by lower $^{87}Sr/^{86}Sr$ values with greater depths. Although the metamorphic sole contains meta-basalts and what appear to be volcanoclastic sediments (Boudier et al., 1988; Kotowski et al., 2021; M. P. Searle & Malpas, 1980, 1982), all of the samples have higher $^{87}Sr/^{86}Sr$ than typical mid-ocean ridge basalts (MORB) (Gale et al., 2013; Hofmann, 2013). The Sr isotope values of the listvenite and serpentinite samples from BT1B are similar to those of listvenites in nearby outcrops (Falk and Kelemen, 2015, Figure 2), which are significantly more radiogenic than $^{87}Sr/^{86}Sr$ values of Oman peridotites (Gerbert-Gaillard, 2002; Lanphere et al., 1981; McCulloch et al., 1981) and Cretaceous to modern seawater (McArthur et al. 2001), but less radiogenic than some Hawasina and autochthonous sediments (Weyhenmeyer, 2000). Our samples of the Hawasina sediments, and those collected from the same region by

Falk and Kelemen (2015) have $^{87}Sr/^{86}Sr$ values ranging from 0.7082 to 0.7241. Six of these Hawasina samples are more radiogenic than any of the samples from Hole BT1B (Figure 2).

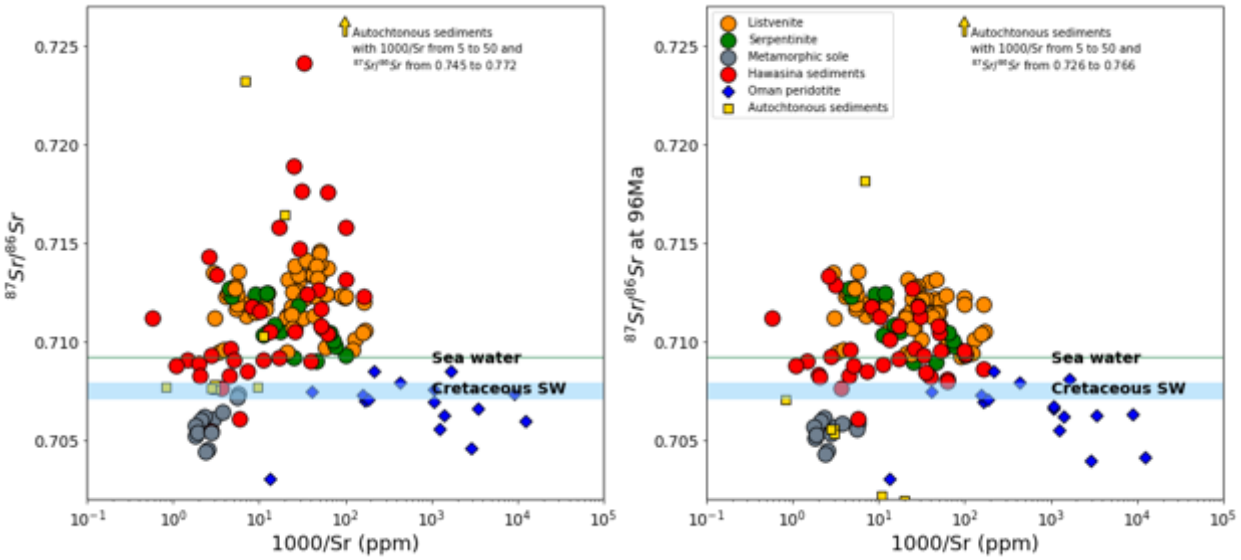

Figure 2. Measured (left) and age corrected at 96Ma (right) Sr isotope ratios and Sr concentrations for core samples from Oman DP Hole BT1B (large circles) compared to Sr isotope ratios in other lithologies measured in Oman. Hawasina sediments from this study and Falk and Kelemen (2015), leached peridotites from Gerbert-Gaillard (2002) and autochthonous sediment samples from Weyhenmeyer (2000). Rb concentrations were not reported for the autochthonous clastic metasediments, so an estimated upper bound Rb concentration of 200 ppm was used.

3.2 Carbon concentrations and $\delta^{13}C$

3.2.1 Total Carbon

The carbon contents of samples from Hole BT1B are highly dependent on lithology (Figure 3). All samples of ultramafic origin contain some carbon, mainly as Mg-rich carbonates, with serpentinites containing 0.2 to 5 wt% carbon, and listvenites containing 6 to 12 wt%. Samples from the metamorphic sole below 200 m depth contain 0.02 to 0.27 wt% carbon. In contrast, the Hawasina sediments have highly variable carbon contents. Some are almost pure metamorphosed limestones and dolomites with carbon contents of up to 11 wt%, while some have less than 0.05 wt% carbon.

$\delta^{13}C$ in the upper 200m of Hole BT1B varies significantly between serpentinites and listvenites (Figure 1). Serpentinites contain significantly lighter carbon than listvenites, as observed in the depth profile (Figure 1). The lower serpentinite band contains two samples (74-2 0.0-5.0 cm and 74-3 42.0-47.0 cm) that contain significantly lighter carbon than any serpentinite in the upper band. In general, carbon concentrations correlate positively with $\delta^{13}C$ values in the upper 200 m (Figure 3). Total carbon $\delta^{13}C$ values in the Hawasina nappes range from -5.52‰ to

229 3.69‰, which almost encompasses the entire range of variation observed in Hole BT1B and
230 appears to decrease with lower carbon contents.

231 ***3.2.2*** *Organic carbon*

232 Graphitic carbon was identified in the core both at the drill site and during core
233 inspection aboard the D/V Chikyu (Kelemen et al, 2020, Kelemen et al. 2021). This organic
234 component has a characteristic low $\delta^{13}C$ signature in listvenites and serpentinites from Hole
235 BT1B, which extends to a minimum of -27.04‰, representing 0.05wt% of total carbon in the
236 sample from 74-1 56.0-64.0cm (Figure 3). In some cases, the intermediate values likely represent
237 mixtures of organic and inorganic carbon, as some of the magnesite in the listvenites is very
238 resistant to 3N HCl attack and remain undissolved even after 5 days of leaching. The observed
239 light isotopic compositions are similar to those observed in other ultramafic localities such as
240 Cerro de Almirez and Liguria (Alt et al. 2013). These data confirm the presence of organic

carbon in Hole BT1B, which was observed during drilling operations, core description aboard D/V Chikyu and via Raman spectroscopy (Kelemen et al, 2020, Kelemen et al. 2021).

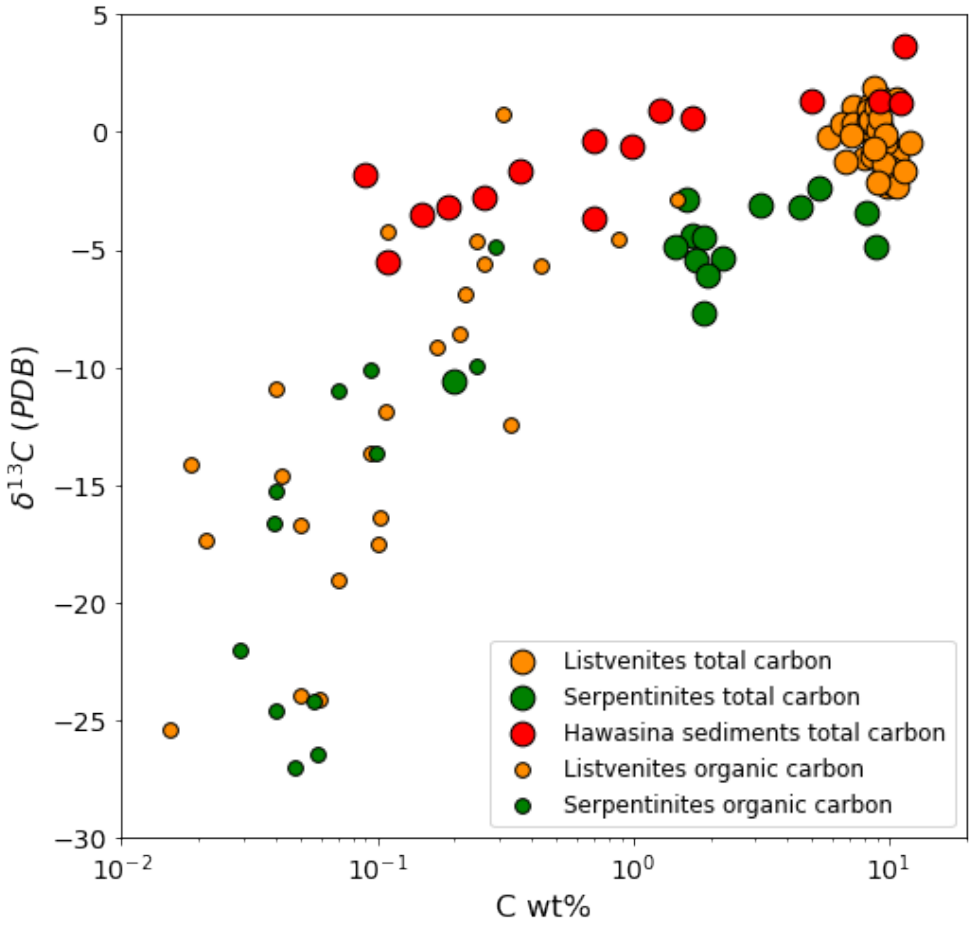

Figure 3. Total carbon and Total Organic Carbon (TOC) vs $\delta^{13}C$ for listvenites, serpentinites and Hawasina sediments.

4 Discussion

4.1 Temperature and pressure of listvenite formation

Falk and Kelemen (2015) estimated the temperature range of listvenite formation based on conventional and clumped stable isotope thermometry (90±15°C), phase equilibria (80-130°C), and rock textures. New clumped isotope measurements on BT1B drill core samples by Beinlich et al. (2020) widened the temperature range of listvenite formation and/or cooling from ~ 50±5 °C to 250±50 °C. This range of values suggests that the infiltrating reactive fluids had variable temperatures, and/or clumped isotope values were reset during cooling, as proposed for fine-grained samples of peridotite-hosted carbonate veins (Garcia del Real et al., 2016). The pressure of listvenite formation is very poorly constrained due to the lack of pressure-sensitive assemblages and the small size of fluid inclusions. A minimum pressure of 0.3 GPa is provided by the P-T conditions recorded by the carbonate platform during ophiolite obduction (Grobe et

al., 2019). For the upper limit, the listvenites must have formed at a pressure below the maximum pressure reported for the metamorphic sole (~ 1.4 GPa) (Cowan et al., 2014; Searle and Cox, 2002).

4.2 Timing of listvenite formation

Falk and Kelemen (2015) used Rb/Sr and $^{87}Sr/^{86}Sr$ data on mineral separates to produce an imprecise isochron age of 97±29Ma for a listvenite sample. This age is broadly consistent with the ~96 Ma age of formation of igneous crust in the ophiolite, along with the same age of metamorphism for the underlying metamorphic sole just beneath the basal thrust of the ophiolite (Hacker, 1994; Hacker et al., 1996; Rioux et al., 2013**,** 2016**)**. Moreover, listvenites are found in and near the basal thrust, from the UAE near the northwestern end of the ophiolite outcrop to the area around Hole BT1B, near the southeastern end of the ophiolite outcrop in Oman (Nasir et al., 2007; Stanger, 1985). The extensive outcrop NE of Hole BT1B, known informally as MoD Mountain, exposes the Banded Horizon, a peridotite unit found at the base of the ophiolite mantle section composed of alternating 1- to 10-meter scale bands of dunite, harzburgite, and minor lherzolite. This unit has distinct geochemical characteristics, with higher Al and middle rare-earth-elements, compared to the residual mantle harzburgites that comprise most of the mantle section of the ophiolite (Boudier et al., 1988; Khedr et al., 2014; Prigent et al., 2018; Yoshikawa et al., 2015).

Tabular listvenites parallel to the dunite-harzburgite banding replace the Banded Unit, at and above the basal thrust. In this region, there is a consistent "stratigraphy" with peridotite (± listvenite) overlying the metamorphic sole, which in turn overlies the allochthonous Hawasina nappe. This stratigraphy is nearly flat-lying, forming a broad anticline with a NW trending hinge near the summit ridge of MoD Mountain, and a broad syncline that is coincident with the valley north of MoD Mountain. Throughout this region, the contacts of listvenite bands within and at the base of the Banded Unit are broadly parallel to banding in the peridotite, and to the contacts between listvenite, peridotite, metamorphic sole, and the Hawasina nappe. These data are consistent with our hypothesis that most of the listvenites formed by alteration of mantle peridotite during the subduction of the underlying sediments via intra-oceanic thrusting and/or later emplacement of the ophiolite onto the Arabian continental margin.

However, some of the listvenites formed or were modified during later events. The basal thrust of the ophiolite was regionally reactivated – mainly with normal sense displacements – during uplift and extension of the Jebel Akdar and Saih Hatat anticlinoria (Cawood et al., 1990; Coffield, 1990; Hanna, 1990; Mattern & Scharf, 2018). Some or all of the cataclasites in BT1B core and surrounding outcrops postdate listvenite formation and may record brittle deformation associated with this reactivation (M.D. Menzel et al., 2020). In turn, the listvenite cataclasites are fine-grained, indurated rocks – hard to drill or sample – that are cut by late, calcite and dolomite rich veins. Thus, it is clear that local fluid-rock interaction of the listvenites continued after brittle deformation.

On the basis of steep, fault-bounded contacts of listvenite with young, post-emplacement conglomerates, several workers have inferred that the listvenites formed during later uplift and extension (Nasir et al., 2007; Stanger, 1985; Wilde et al., 2002). Recently, Scharf et al. (2020) reported 60 ± 16 Ma and 58 ± 6 Ma U/Pb ages for two carbonate veins that cut listvenite, and

300 structural observations indicating a top-down sense of shear along some faulted listvenite-
301 peridotite and listvenite-sole contacts. Following prior interpretations, they interpret these ages
302 as formation ages of the listvenites after ophiolite emplacement during uplift of the nearby Jebel
303 Akdar and Saih Hatat anticlinoria. We find that their interpretation is inconsistent with the field
304 observations reported above.

305 We have age-corrected our $^{87}Sr/^{86}Sr$ to the 96 Ma age reported by Falk and Kelemen
306 (2015). This correction gives the lowest possible $^{87}Sr/^{86}Sr$ for all the samples based on reported
307 ages. For the corrections, we used Sr and Rb concentrations reported by Godard et al.
308 (submitted) for Hole BT1B and our analyses of Hawasina sediments. While Rb/Sr is low in most
309 BT1B samples and thus age corrections are small, this correction removes some of the apparent
310 trends observed in measured $^{87}Sr/^{86}Sr$ versus depth. The age corrections particularly affect
311 listvenites with relatively abundant chromian mica (fuchsite-muscovite solid solutions, Falk &
312 Kelemen 2015, supplement) in the 115-163 m depth interval, as these micas host abundant Rb
313 (Godard et al. submitted). The age correction also affects the estimated $^{87}Sr/^{86}Sr$ values of the
314 metamorphic sole of BT1B and some of the Hawasina sediments as their Sr and Rb
315 concentrations are heterogeneous, ranging from 9 to 638 ppm for Sr and 0.4 to 97.7 ppm for Rb.
316 Regardless, the age-corrected $^{87}Sr/^{86}Sr$ values of the listvenites are much higher than those of the
317 mantle and Cretaceous seawater. The only plausible source of this radiogenic Sr is from the
318 underlying Hawasina sediments.

319 *4.3 Fluid source for carbonation of peridotites in Oman DP Hole BT1B*

320 $^{87}Sr/^{86}Sr$ and $d^{13}C$ data on MoD Mountain listvenites and Hole BT1B samples suggest
321 that replacement of peridotite by serpentinite and listvenite resulted from reaction with a single
322 fluid along a reaction path (Kelemen et al. 2021). The initial fluid was far from equilibrium with
323 peridotite, which converted olivine and serpentine in the protolith to carbonates + quartz and
324 approached equilibrium with serpentinite at higher extents of reaction progress and lower
325 integrated water/rock ratios (Beinlich et al 2020, Kelemen et al. 2021). Mg isotope data from a
326 set of samples studied by Falk and Kelemen (2015) show significant differences between
327 dolomite and magnesite listvenites. Dolomite listvenites (average $\delta^{26}Mg \sim -1.33$) are lighter in
328 Mg isotopes than magnesite listvenites (average $\delta^{26}Mg \sim -0.33$) (de Obeso et al., 2021), which
329 suggests magnesite dissolution and dolomite formation. This is consistent with the modelled
330 evolution of listvenites during fluid-rock reaction, with dolomite replacing magnesite at
331 increasing water/rock ratios (Kelemen et al. 2021).

332 As noted above, after the magnesite and dolomite listvenites formed they were
333 cataclastically deformed, and then cut by late Ca-rich carbonate veins (Menzel et al. 2020). Thus,
334 one might expect the veins to have formed from a later, geochemically distinctive fluid as
335 suggested by variable clumped isotope ($\Delta 47$) derived temperatures (Beinlich et al., 2020). This
336 can be addressed in future studies via careful sampling of the post-cataclastic veins.

337 Returning attention to the source of the fluid that formed the bulk of the listvenites,
338 assuming that Sr and CO_2 were derived from the same fluid, Sr isotopes can be used to constrain
339 the source of the carbonating fluids that formed the serpentinites and listvenites. Falk and
340 Kelemen (2015) proposed three possible sources of fluids for carbonation: (1) compaction of
341 pore waters from underlying Hawasina sediments, (2) low temperature dehydration of opal and

clay minerals in calcite-bearing Hawasina sediments, and (3) higher-grade metamorphic devolatilization reactions involving subducted sediments similar to the Hawasina sediments coupled with fluid that migrated up the subduction zone.

Unlike younger, mantle-peridotite-hosted carbonates, the listvenites do not contain a significant fraction of seawater- or groundwater-derived Sr. The listvenites have $^{87}Sr/^{86}Sr$ ratios that are distinct from recent, low-temperature carbonate veins and travertine in the mantle section of the ophiolite (de Obeso & Kelemen, 2018; Peter B. Kelemen et al., 2011; Weyhenmeyer, 2000). Almost all of the listvenites and associated serpentinites from BT1B core and MoD Mountain outcrops have $^{87}Sr/^{86}Sr$ ratios at 96 Ma higher than Cretaceous seawater (Falk & Kelemen 2015, and this paper). In contrast, young, peridotite-hosted carbonate veins and travertines in the Samail ophiolite consistently have $^{87}Sr/^{86}Sr$ lower than 0.709 and appear to contain mixtures of Sr derived from seawater or groundwater and the mantle (de Obeso & Kelemen, 2018; Gerbert-Gaillard, 2002; Peter B. Kelemen et al., 2011; Weyhenmeyer, 2000).

In addition, the listvenites do not contain significant Sr from the metamorphic sole sampled in Hole BT1B. Core samples of the sole have $^{87}Sr/^{86}Sr$ ratios that are similar to Indian Ocean MORB and near-ridge Pacific seamounts (Hofmann, 2013), which are systematically lower than the Sr isotope ratios of the listvenites. Perhaps the metabasalts are remnants of a subducted seamount, similar to accreted seamounts along the Cascadia margin of North America (e.g., Duncan, 1982), which derived from the enriched mantle source of some Indian Ocean MORB. Alternatively, the $^{87}Sr/^{86}Sr$ ratios may have increased during alteration.

In contrast, age-corrected Sr isotope ratios for Hawasina sediments underlying the ophiolite and the metamorphic sole, north and northeast of Hole BT1B, have $^{87}Sr/^{86}Sr$ up to 0.7134 at 96 Ma (Figure 2). The samples with the most radiogenic $^{87}Sr/^{86}Sr$ are clastic sediments containing minor amounts of carbonates. Hawasina limestones, on the other hand, have lower $^{87}Sr/^{86}Sr$ values, which is consistent with calcite precipitated from seawater that incorporated a minor, radiogenic clastic component. Based on these observations, the most likely source of the fluids that formed the listenvites are derived from the Hawasina sediments.

Thermodynamic modeling of fluid-rock reactions (Kelemen et al. 2021) shows that the characteristic listvenite mineral assemblages – magnesite + quartz – are attained from fluids with ~ 20,000 ppm dissolved C for listvenite formation at 100-300 °C and 0.5 to 1 GPa, similar to the assemblages modeled by Klein and Garrido (2011) at lower pressures. Such high dissolved carbon contents are impossible to attain by congruent dissolution of pure calcite in aqueous fluids at these P-T conditions (Peter B. Kelemen & Manning, 2015), which rules out silicate-poor limestones such as those from the continental margin as a carbon source. On the other hand, metamorphic devolatilization of rocks composed of silicate-carbonate mixtures can produce C-rich fluids at temperatures above 400 °C and low to moderate pressures, depending on the rock composition. Thus, we infer that the fluids that formed the listvenites derived from devolatilization of subducting metasediments. During prograde subduction metamorphism, calc-silicate rocks, containing both clastic and carbonate components, undergo extensive devolatilization at 2-3 GPa and 500 to 700°C (Gorman et al., 2006; Stewart & Ague, 2020) and

lose significant amounts of their CO_2 in this PT range due to reactions similar to the simplified reaction:

$$CaMg(CO_3)_2 \text{ (dolomite)} + CaMgSi_2O_6 \text{ (diopside)} + 2\ CaAl_2Si_2O_7(OH)_2 \cdot H_2O \text{ (lawsonite)}$$

$$= 2\ Ca_2MgAl_2Si_3O_{12} \text{ (garnet)} + 4\ H_2O + 2\ CO_2$$

In contrast, carbonate-rich compositions (limestone, dolomite, marble) are predicted to retain most of their CO_2 during subduction (e.g, (Kerrick & Connolly, 2001; Stewart & Ague, 2020)).

At temperatures greater than ~ 300°C, dissolved CO_2 in aqueous fluids have $\delta^{13}C$ values that are higher than those of co-existing calcite and dolomite (Chacko et al., 1991; Deines, 2004; Horita, 2014). Thus, for example, fluid in equilibrium with calcite with $\delta^{13}C$ between -4‰ to -6‰ (as in Hawasina clastic sediments) would contain dissolved CO_2 with $\delta^{13}C$ of -2.3‰ to -0.3‰ at 500°C. At lower temperatures, like those estimated for listvenite formation, calcite and dolomite have $\delta^{13}C$ higher than co-existing fluids. Thus, dolomite and presumably magnesite in equilibrium with fluids with $\delta^{13}C$ of -2.3‰ to -0.3‰ would have $\delta^{13}C$ in the range of -0.9‰ to 1.1‰, similar to the $\delta^{13}C$ observed in the listvenites from Hole BT1B and the surrounding outcrops.

Figure 4a illustrates that the listvenites and serpentinites from Hole BT1B lie along the reaction path proposed by Kelemen et al. (2021) at 200°C and 0.5GPa that forms listvenites with W/R~100. In our calculations, we assume that reacting fluids enriched in Sr (250 ppm) with $^{87}Sr/^{86}Sr$ values @96Ma that are similar to those of clastic Hawasina metasediments (0.7110 to 0.7135) reacted with the peridotite with mantle-like $^{87}Sr/^{86}Sr$ (0.7027±0.0011). The listvenites and serpentinites follow a mixing trend (Figure 4b) between mantle peridotite like compositions (Sr=1.5 ppm, $^{87}Sr/^{86}Sr$=0.7027±0.0011, C=680ppm and $\delta^{13}C$=6.0±2.0‰) and low temperature carbonates that crystallized from a fluid produced by high-pressure, high-temperature devolatilization with Sr isotope ratios in the range of the Hawasina clastic sediments (Sr=250ppm, $^{87}Sr/^{86}Sr$~0.7100 to 0.7135) and fractionated carbon isotopes as described above. These trends together suggest that the CO_2-bearing aqueous fluids that formed the listvenites from Hole BT1B and surrounding outcrops were derived by devolatilization of calc-silicate metasediments, with $^{87}Sr/^{86}Sr$ and $\delta^{13}C$ similar to clastic sediments in the Hawasina Formation

along a subduction zone geotherm. These fluids migrated up dip to lower pressures and temperatures to form the listvenites.

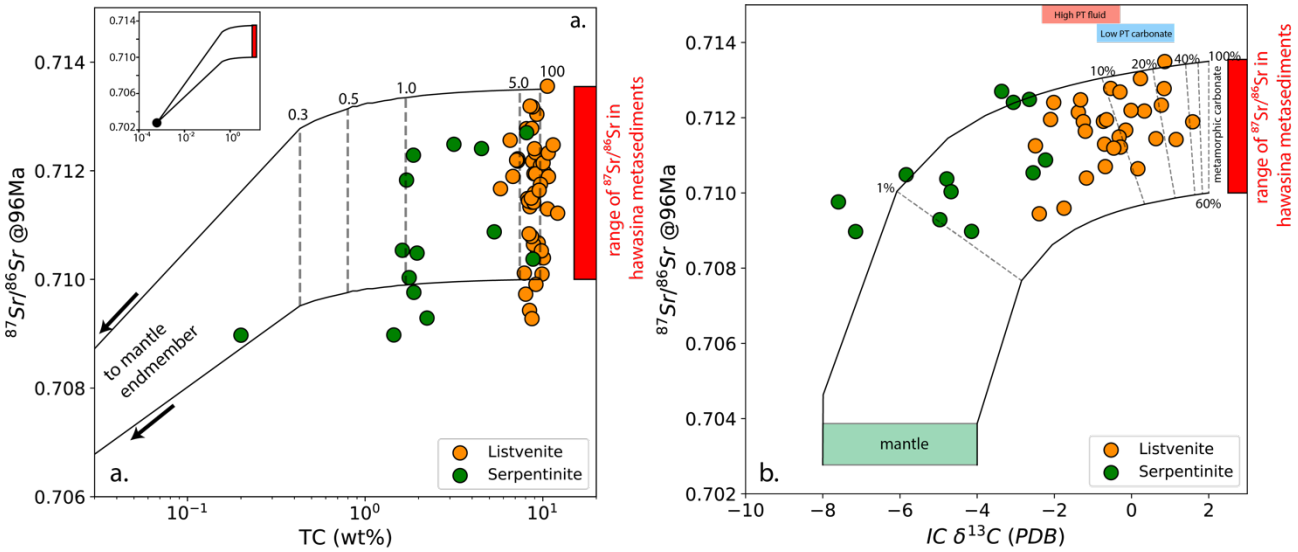

Figure 4. (a. left) Total carbon (wt%) vs $^{87}Sr/^{86}Sr$ @96Ma. Black lines are reaction paths of carbon rich fluid reacting with peridotite at 200°C and 0.5GPa at variable water/rock (tie lines) from Kelemen et al. (submitted). The reacting fluid is assumed to have $^{87}Sr/^{86}Sr$ values of 0.7100 to 0.7135 like those of clastic Hawasina metasediments. (b. right) Inorganic carbon $\delta^{13}C$ vs $^{87}Sr/^{86}Sr$ @96Ma. Black lines are mixing lines between mantle and carbonate minerals precipitated from a metamorphic fluid. The fluid has the same carbon concentration as the reaction path on the figure 4a and the $\delta^{13}C$ fractionation between the carbonate and the fluid are described in the body of the text with values for high and low PT shown top. We assume that the fluid has the Sr isotope ratios of Hawasina clastic sediments. $^{87}Sr/^{86}Sr$ values for the depleted mantle are for mid-ocean-ridge-basalt (MORB) from (Hofmann, 2013) . Mantle $\delta^{13}C$ is from (Deines, 2002).

5 Conclusions

Listvenites and spatially associated serpentinites from Hole BT1B and surrounding outcrops that replace residual mantle peridotites from the base of the Samail ophiolite have Sr isotope ratios that are more radiogenic than their peridotite protoliths, Cretaceous seawater, modern seawater, groundwater in the ophiolite, and the underlying metamorphic sole. We suggest that the radiogenic Sr isotope component was transported via carbon-rich aqueous fluid that reacted with the peridotite to form the listvenites and serpentinites. The $^{87}Sr/^{86}Sr$ values of this component resemble those of calcite-bearing clastic sediments in the Hawasina Formation underlying the ophiolite and the metamorphic sole. However, the fluid must have contained higher dissolved carbon contents than feasible for congruent dissolution of pure calcite at < 2 GPa and/or < 550°C. Thus, we hypothesize that this fluid was derived by devolatilization of carbonate- and silicate bearing meta-sediments akin to the Hawasina clastic sediments at 0.5 to 2.3 GPa and 400 to 700°C in the subduction zone (M. P. Searle et al., 1994). This fluid then migrated up dip to

react with hanging wall peridotite at <1 GPa and <250°C, forming the listvenites and serpentinites. Carbon isotope fractionation during high temperature devolatilization followed by low temperature carbonate precipitation during the reaction with peridotite likely controlled the isotopic characteristics of the listvenites and the serpentinites with $\delta^{13}C$ from -10.6‰ to 1.92‰ and $^{87}Sr/^{86}Sr$ from 0.7090 to 0.7145.

6 Acknowledgments and Data

Juan Carlos de Obeso wants to thank Steven Goldstein for allowing early access to the laboratories in LDEO to complete isotope work soon after partial reopening following the first wave of the COVID-19 pandemic in New York. Wei Huang is thanked for help with measurements of carbon concentrations and δ13C. This research used samples and/or data provided by the Oman Drilling Project. The Oman Drilling Project (OmanDP) has been possible through co-mingled funds from the International Continental Scientific Drilling Project (ICDP; Kelemen, Matter, Teagle Lead PIs), the Sloan Foundation – Deep Carbon Observatory (Grant 2014-3-01, Kelemen PI), the National Science Foundation (NSF-EAR-1516300, Kelemen lead PI), NASA – Astrobiology Institute (NNA15BB02A, Templeton PI), the German Research Foundation (DFG: KO 1723/21-1, Koepke PI), the Japanese Society for the Promotion of Science (JSPS no:16H06347, Michibayashi PI; and KAKENHI 16H02742, Takazawa PI), the European Research Council (Adv: no.669972; Jamveit PI), the Swiss National Science Foundation (SNF:20FI21_163073, Früh-Green PI), JAMSTEC, the TAMU-JR Science Operator, and contributions from the Sultanate of Oman Ministry of Regional Municipalities and Water Resources, the Oman Public Authority of Mining, Sultan Qaboos University, CNRS-Univ. Montpellier, Columbia University of New York, and the University of Southampton.

Authors declare no conflict of interest.

All data will be uploaded to EarthChem or a similar repository prior to final publication.

7 References

Alt, J. C., Schwarzenbach, E. M., Früh-Green, G. L., Shanks, W. C., Bernasconi, S. M., Garrido, C. J., Crispini, L., Gaggero, L., Padrón-Navarta, J. A., & Marchesi, C. (2013). The role of serpentinites in cycling of carbon and sulfur: Seafloor serpentinization and subduction metamorphism. *Lithos*, *178*, 40–54. https://doi.org/10.1016/j.lithos.2012.12.006

Bach, W., Rosner, M., Jöns, N., Rausch, S., Robinson, L. F., Paulick, H., & Erzinger, J. (2011). Carbonate veins trace seawater circulation during exhumation and uplift of mantle rock: Results from ODP Leg 209. *Earth and Planetary Science Letters*, *311*(3–4), 242–252. https://doi.org/10.1016/j.epsl.2011.09.021

Bechennec, F., Le Metour, J., Rabu, D., Bourdillon-de-Grissac, C., de Wever, P., Beurrier, M., & Villey, M. (1990). The Hawasina Nappes: Stratigraphy, palaeogeography and structural evolution of a fragment of the south-Tethyan passive continental margin. *Geological Society Special Publication*, *49*(49), 213–223.

https://doi.org/10.1144/GSL.SP.1992.049.01.14

Béchennec, F., Le Métour, J., Rabu, D., Villey, M., & Beurrier, M. (1988). The Hawasina Basin: A fragment of a starved passive continental margin, thrust over the Arabian Platform during obduction of the Sumail Nappe. *Tectonophysics*, *151*(1–4). https://doi.org/10.1016/0040-1951(88)90251-X

Beinlich, A., Pl??mper, O., H??velmann, J., Austrheim, H., & Jamtveit, B. (2012). Massive serpentinite carbonation at Linnajavri, N-Norway. *Terra Nova*, *24*(6), 446–455. https://doi.org/10.1111/j.1365-3121.2012.01083.x

Beinlich, A., Plümper, O., Boter, E., Müller, I. A., Kourim, F., Ziegler, M., Harigane, Y., Lafay, R., & Kelemen, P. B. (2020). Ultramafic Rock Carbonation: Constraints From Listvenite Core BT1B, Oman Drilling Project. *Journal of Geophysical Research: Solid Earth*, *125*(6), 1–21. https://doi.org/10.1029/2019jb019060

Blakely, R. J., Brocher, T. M., & Wells, R. E. (2005). Subduction-zone magnetic anomalies and implications for hydrated forearc mantle. *Geology*, *33*(6), 445–448. https://doi.org/10.1130/G21447.1

Boskabadi, A., Pitcairn, I. K., Broman, C., Boyce, A., Teagle, D. A. H., Cooper, M. J., Azer, M. K., Stern, R. J., Mohamed, F. H., & Majka, J. (2017). Carbonate alteration of ophiolitic rocks in the Arabian–Nubian Shield of Egypt: sources and compositions of the carbonating fluid and implications for the formation of Au deposits. *International Geology Review*, *59*(4), 391–419. https://doi.org/10.1080/00206814.2016.1227281

Boskabadi, A., Pitcairn, I. K., Leybourne, M. I., Teagle, D. A. H., Cooper, M. J., Hadizadeh, H., Nasiri Bezenjani, R., & Monazzami Bagherzadeh, R. (2020). Carbonation of ophiolitic ultramafic rocks: Listvenite formation in the Late Cretaceous ophiolites of eastern Iran. *Lithos*, *352–353*, 105307. https://doi.org/10.1016/j.lithos.2019.105307

Boudier, F., Ceuleneer, G., & Nicolas, A. (1988). Shear zones, thrusts and related magmatism in the Oman ophiolite: Initiation of thrusting on an oceanic ridge. *Tectonophysics*, *151*(1–4), 275–296. https://doi.org/10.1016/0040-1951(88)90249-1

Braun, M. G. (2004). *Petrologic and Microstructural Constraints on Focused Melt Transport in Dunites and Rheology of the Shallow Mantle* [WHOI/MIT]. http://oai.dtic.mil/oai/oai?verb=getRecord&metadataPrefix=html&identifier=ADA426948

Braun, M. G., & Kelemen, P. B. (2002). Dunite distribution in the Oman Ophiolite: Implications for melt flux through porous dunite conduits. *Geochemistry, Geophysics, Geosystems*, *3*(11), 1–21. https://doi.org/10.1029/2001GC000289

Cawood, P. A., Green, F. K., & Calon, T. J. (1990). Origin of culminations within the Southeast Oman Mountains at Jebel Ma-jhool and Ibra Dome. *Geological Society, London, Special Publications*, *49*(1), 429–445. https://doi.org/10.1144/GSL.SP.1992.049.01.27

Chacko, T., Mayeda, T. K., Clayton, R. N., & Goldsmith, J. R. (1991). Oxygen and carbon isotope fractionations between CO2 and calcite. *Geochimica et Cosmochimica Acta*, *55*(10), 2867–2882. https://doi.org/10.1016/0016-7037(91)90452-B

Clark, I. D., & Fontes, J.-C. (1990). Paleoclimatic reconstruction in northern Oman based on carbonates from hyperalkaline groundwaters. *Quaternary Research*, *33*(3), 320–336.

https://doi.org/10.1016/0033-5894(90)90059-T

Coffield, D. Q. (1990). Structures associated with nappe emplacement and culmination collapse in the Central Oman Mountains. *Geological Society, London, Special Publications*, *49*(1), 447–458. https://doi.org/10.1144/GSL.SP.1992.049.01.28

Collier, M. L. (2012). *Spatial-Statistical Properties of Geochemical Variability as Constraints on Magma Transport and Evolution Processes at Ocean Ridges*. Columbia University.

Cowan, R. J., Searle, M. P., & Waters, D. J. (2014). Structure of the metamorphic sole to the Oman Ophiolite, Sumeini Window and Wadi Tayyin: Implications for ophiolite obduction processes. *Geological Society Special Publication*, *392*(1), 155–175. https://doi.org/10.1144/SP392.8

de Obeso, J. C., & Kelemen, P. B. (2018). Fluid rock interactions on residual mantle peridotites overlain by shallow oceanic limestones: Insights from Wadi Fins, Sultanate of Oman. *Chemical Geology*. https://doi.org/10.1016/J.CHEMGEO.2018.09.022

de Obeso, J. C., & Kelemen, P. B. (2020). Major element mobility during serpentinization, oxidation and weathering of mantle peridotite at low temperatures. *Philosophical Transactions. Series A, Mathematical, Physical, and Engineering Sciences*, *378*(2165), 20180433. https://doi.org/10.1098/rsta.2018.0433

de Obeso, J. C., Santiago Ramos, D. P., Higgins, J. A., & Kelemen, P. B. (2021). A Mg Isotopic Perspective on the Mobility of Magnesium During Serpentinization and Carbonation of the Oman Ophiolite. *Journal of Geophysical Research: Solid Earth*, *126*(2), 1–17. https://doi.org/10.1029/2020JB020237

Deines, P. (2002). The carbon isotope geochemistry of mantle xenoliths. *Earth-Science Reviews*, *58*(3–4), 247–278. https://doi.org/10.1016/S0012-8252(02)00064-8

Deines, P. (2004). Carbon isotope effects in carbonate systems. *Geochimica et Cosmochimica Acta*, *68*(12), 2659–2679. https://doi.org/10.1016/j.gca.2003.12.002

Delacour, A., Früh-Green, G. L., Bernasconi, S. M., Schaeffer, P., & Kelley, D. S. (2008). Carbon geochemistry of serpentinites in the Lost City Hydrothermal System (30°N, MAR). *Geochimica et Cosmochimica Acta*, *72*(15), 3681–3702. https://doi.org/10.1016/J.GCA.2008.04.039

DeShon, H. R., & Schwartz, S. Y. (2004). Evidence for serpentinization of the forearc mantle wedge along the Nicoya Peninsula, Costa Rica. *Geophysical Research Letters*, *31*(21), 2–5. https://doi.org/10.1029/2004GL021179

Falk, E. S., & Kelemen, P. B. (2015). Geochemistry and petrology of listvenite in the Samail ophiolite, Sultanate of Oman: Complete carbonation of peridotite during ophiolite emplacement. *Geochimica et Cosmochimica Acta*, *160*, 70–90. https://doi.org/10.1016/j.gca.2015.03.014

Fruh-Green, G. L., Connolly, J. A. D. D., Plas, A., Kelley, D. S., Grobety, B., Früh-Green, G. L., Connolly, J. A. D. D., Plas, A., Kelley, D. S., & Grobéty, B. (2004). Serpentinization of oceanic peridotites: Implications for geochemical cycles and biological activity. In *AGU Monograph* (Vol. 144, pp. 119–136). https://doi.org/10.1029/144GM08

Gale, A., Dalton, C. A., Langmuir, C. H., Su, Y., & Schilling, J. G. (2013). The mean

composition of ocean ridge basalts. *Geochemistry, Geophysics, Geosystems*, *14*(3), 489–518. https://doi.org/10.1029/2012GC004334

Garcia del Real, P., Maher, K., Kluge, T., Bird, D. K., Brown, G. E., & John, C. M. (2016). Clumped-isotope thermometry of magnesium carbonates in ultramafic rocks. *Geochimica et Cosmochimica Acta*, *193*, 222–250. https://doi.org/10.1016/j.gca.2016.08.003

Gerbert-Gaillard, L. (2002). *Caractérisation Géochimique des Péridotites de l'ophiolite d'Oman : processus magmatiques aux limites lithosphère/asthenosphère*. Université Montpellier II - Sciences et Techniques du Languedoc.

Godard, M., Jousselin, D., & Bodinier, J.-L. (2000). Relationships between geochemistry and structure beneath a palaeo-spreading centre: a study of the mantle section in the Oman ophiolite. *Earth and Planetary Science Letters*, *180*(1–2), 133–148. https://doi.org/10.1016/S0012-821X(00)00149-7

Gorman, P. J., Kerrick, D. M., & Connolly, J. a. D. (2006). Modeling open system metamorphic decarbonation of subducting slabs. *Geochemistry, Geophysics, Geosystems*, *7*(4). https://doi.org/10.1029/2005GC001125

Grobe, A., Von Hagke, C., Littke, R., Dunkl, I., Wübbeler, F., Muchez, P., & Urai, J. L. (2019). Tectono-Thermal evolution of Oman's Mesozoic passive continental margin under the obducting Semail Ophiolite: A case study of Jebel Akhdar, Oman. *Solid Earth*, *10*(1), 149–175. https://doi.org/10.5194/se-10-149-2019

Hacker, B. R. (1994). Rapid Emplacement of Young Oceanic Lithosphere: Argon Geochronology of the Oman Ophiolite. *Science*, *265*(5178), 1563–1565. https://doi.org/10.1126/science.265.5178.1563

Hacker, B. R., & Mosenfelder, J. L. (1996). Metamorphism and deformation along the emplacement thrust of the Samail ophiolite, Oman. *Earth and Planetary Science Letters*, *144*(3–4), 435–451. https://doi.org/10.1016/S0012-821X(96)00186-0

Hacker, B. R., Mosenfelder, J. L., & Gnos, E. (1996). Rapid emplacement of the Oman ophiolite: Thermal and geochronologic constraints. *Tectonics*, *15*(6), 1230–1247. https://doi.org/10.1029/96TC01973

Hanghøj, K., Kelemen, P. B., Hassler, D., & Godard, M. (2010). Composition and Genesis of Depleted Mantle Peridotites from the Wadi Tayin Massif, Oman Ophiolite; Major and Trace Element Geochemistry, and Os Isotope and PGE Systematics. *Journal of Petrology*, *51*(1–2), 201–227. https://doi.org/10.1093/petrology/egp077

Hanna, S. S. (1990). The Alpine deformation of the Central Oman Mountains. *Geological Society, London, Special Publications*, *49*(1), 341–359. https://doi.org/10.1144/GSL.SP.1992.049.01.21

Hansen, L. D., Dipple, G. M., Gordon, T. M., & Kellett, D. a. (2005). Carbonated Serpentinite (Listwanite) At Atlin, British Columbia: a Geological Analogue To Carbon Dioxide Sequestration. *The Canadian Mineralogist*, *43*(1), 225–239. https://doi.org/10.2113/gscanmin.43.1.225

Hofmann, A. W. (2013). Sampling Mantle Heterogeneity through Oceanic Basalts: Isotopes and Trace Elements. In *Treatise on Geochemistry: Second Edition* (2nd ed., Vol. 3, Issue 1968).

Elsevier Ltd. https://doi.org/10.1016/B978-0-08-095975-7.00203-5

Horita, J. (2014). Oxygen and carbon isotope fractionation in the system dolomite-water-CO2 to elevated temperatures. *Geochimica et Cosmochimica Acta*, *129*, 111–124. https://doi.org/10.1016/j.gca.2013.12.027

Hyndman, R. D., & Peacock, S. M. (2003). Serpentinization of the forearc mantle. *Earth and Planetary Science Letters*, *212*(3–4), 417–432. https://doi.org/10.1016/S0012-821X(03)00263-2

Kamiya, S., & Kobayashi, Y. (2000). Seismological evidence for the existence of serpentinized wedge mantle. *Geophysical Research Letters*, *27*(6), 819–822. https://doi.org/10.1029/1999GL011080

Kelemen, P.B., Matter, J. M., Teagle, D. A. H., & Coggon, J. A. (Eds.). (2020). *Proceedings of the Oman Drilling Project: Vol. Phase 1 an*. International Ocean Discovery Program. https://doi.org/10.14379/OmanDP.proc.2020

Kelemen, Peter B., de Obeso, J. C., Leong, J. A. M., Godard, M., Okazaki, K., Kotowski, A. J., Manning, C. E., Ellison, E. T., Menzel, M. D., Urai, J. L., Hirth, G., Rioux, M., Stockli, D. F., Lafay, R., Beinlich, A., Coggon, J., Warsi, N. H., Matter, J. M., Teagle, D. A. H., … Harris, M. (2021). Mass transfer into the leading edge of the mantle wedge: Initial results from Oman Drilling Project Hole BT1B. *Earth and Space Science Open Archive*. https://doi.org/10.1002/essoar.10507370.1

Kelemen, Peter B., & Manning, C. E. (2015). Reevaluating carbon fluxes in subduction zones, what goes down, mostly comes up. *Proceedings of the National Academy of Sciences*, *112*(30), E3997–E4006. https://doi.org/10.1073/pnas.1507889112

Kelemen, Peter B., & Matter, J. M. (2008). In situ carbonation of peridotite for CO2 storage. *Proceedings of the National Academy of Sciences*, *105*(45), 17295–17300. https://doi.org/10.1073/pnas.0805794105

Kelemen, Peter B., Matter, J. M., Streit, E. E., Rudge, J. F., Curry, W. B., & Blusztajn, J. (2011). Rates and Mechanisms of Mineral Carbonation in Peridotite: Natural Processes and Recipes for Enhanced, in situ CO 2 Capture and Storage. *Annual Review of Earth and Planetary Sciences*, *39*(1), 545–576. https://doi.org/10.1146/annurev-earth-092010-152509

Kelemen, Peter B., Matter, J. M., Teagle, D. A. H., Coggon, J. A., & The Oman Drilling Project Science. (2020). Site BT1: fluid and mass exchange on a subduction zone plate boundary. In Peter B. Kelemen, J. M. Matter, D. A. H. Teagle, J. A. Coggon, & et al. (Eds.), *Proceedings of the Oman Drilling Project*. International Ocean Discovery Program.

Kerrick, D. M., & Connolly, J. A. D. (2001). Metamorphic devolatilization of subducted marine sediments and the transport of volatiles into the Earth's mantle. *Nature*, *411*, 293. http://dx.doi.org/10.1038/35077056

Khedr, M. Z., Arai, S., Python, M., & Tamura, A. (2014). Chemical variations of abyssal peridotites in the central Oman ophiolite: Evidence of oceanic mantle heterogeneity. *Gondwana Research*, *25*(3), 1242–1262. https://doi.org/10.1016/J.GR.2013.05.010

Klein, F., Humphris, S. E., & Bach, W. (2020). Brucite formation and dissolution in oceanic serpentinite. *Geochemical Perspectives Letters*, 1–5.

https://doi.org/10.7185/geochemlet.2035

Kotowski, A. J., Cloos, M., Stockli, D. F., & Orent, E. B. (2021). Structural and thermal evolution of an infant subduction shear zone: Insights from sub-ophiolite metamorphic rocks recovered from Oman Drilling Project Site BT-1B. *Earth and Space Science Open Archive*. https://doi.org/https://doi.org/10.1002/essoar.10505943.1

Lanphere, M. A., Coleman, R. G., & Hopson, C. A. (1981). Sr isotopic tracer study of the Samail Ophiolite, Oman. *Journal of Geophysical Research: Solid Earth*, *86*(B4), 2709–2720. https://doi.org/10.1029/JB086iB04p02709

Macdonald, A. H., & Fyfe, W. S. (1985). Rate of serpentinization in seafloor environments. *Tectonophysics*, *116*(1–2), 123–135. https://doi.org/10.1016/0040-1951(85)90225-2

Mattern, F., & Scharf, A. (2018). Postobductional extension along and within the Frontal Range of the Eastern Oman Mountains. *Journal of Asian Earth Sciences*, *154*(September 2017), 369–385. https://doi.org/10.1016/j.jseaes.2017.12.031

McCulloch, M. T., Gregory, R. T., Wasserburg, G. J., & Taylor, H. P. (1981). Sm-Nd, Rb-Sr, and18O/16O isotopic systematics in an oceanic crustal section: evidence from the Samail ophiolite. *Journal of Geophysical Research*, *86*(B4), 2721–2735. https://doi.org/10.1029/JB086iB04p02721

Menzel, M.D., Urai, J. L., de Obeso, J. C., Kotowski, A., Manning, C. E., Kelemen, P. B., Kettermann, M., Jesus, A. P., & Harigane, Y. (2020). Brittle Deformation of Carbonated Peridotite—Insights From Listvenites of the Samail Ophiolite (Oman Drilling Project Hole BT1B). *Journal of Geophysical Research: Solid Earth*, *125*(10). https://doi.org/10.1029/2020JB020199

Menzel, Manuel D., Garrido, C. J., López Sánchez-Vizcaíno, V., Marchesi, C., Hidas, K., Escayola, M. P., & Delgado Huertas, A. (2018). Carbonation of mantle peridotite by CO2-rich fluids: the formation of listvenites in the Advocate ophiolite complex (Newfoundland, Canada). *Lithos*, *323*, 238–261. https://doi.org/10.1016/J.LITHOS.2018.06.001

Monnier, C., Girardeau, J., Le Mée, L., & Polvé, M. (2006). Along-ridge petrological segmentation of the mantle in the Oman ophiolite. *Geochemistry, Geophysics, Geosystems*, *7*(11), n/a-n/a. https://doi.org/10.1029/2006GC001320

Nasir, S., Al Sayigh, A. R., Al Harthy, A., Al-Khirbash, S., Al-Jaaidi, O., Musllam, A., Al-Mishwat, A., & Al-Bu'saidi, S. (2007). Mineralogical and geochemical characterization of listwaenite from the Semail Ophiolite, Oman. *Chemie Der Erde - Geochemistry*, *67*(3), 213–228. https://doi.org/10.1016/j.chemer.2005.01.003

Noël, J., Godard, M., Oliot, E., Martinez, I., Williams, M., Boudier, F., Rodriguez, O., Chaduteau, C., Escario, S., & Gouze, P. (2018). Evidence of polygenetic carbon trapping in the Oman Ophiolite: Petro-structural, geochemical, and carbon and oxygen isotope study of the Wadi Dima harzburgite-hosted carbonates (Wadi Tayin massif, Sultanate of Oman). *Lithos*, *323*, 218–237. https://doi.org/10.1016/J.LITHOS.2018.08.020

Paulick, H., Bach, W., Godard, M., De Hoog, J. C. M., Suhr, G., & Harvey, J. (2006). Geochemistry of abyssal peridotites (Mid-Atlantic Ridge, 15°20′N, ODP Leg 209): Implications for fluid/rock interaction in slow spreading environments. *Chemical Geology*, *234*(3–4), 179–210. https://doi.org/10.1016/j.chemgeo.2006.04.011

Prigent, C., Agard, P., Guillot, S., Godard, M., & Dubacq, B. (2018). Mantle Wedge (De)formation During Subduction Infancy: Evidence from the Base of the Semail Ophiolitic Mantle. *Journal of Petrology*, *59*(11), 2061–2092. https://doi.org/10.1093/petrology/egy090

Quesnel, B., Boulvais, P., Gautier, P., Cathelineau, M., John, C. M., Dierick, M., Agrinier, P., & Drouillet, M. (2016). Paired stable isotopes (O, C) and clumped isotope thermometry of magnesite and silica veins in the New Caledonia Peridotite Nappe. *Geochimica et Cosmochimica Acta*, *183*, 234–249. https://doi.org/10.1016/j.gca.2016.03.021

Rioux, M., Bowring, S., Kelemen, P. B., Gordon, S., Miller, R., & Dudás, F. (2013). Tectonic development of the Samail ophiolite: High-precision U-Pb zircon geochronology and Sm-Nd isotopic constraints on crustal growth and emplacement. *Journal of Geophysical Research: Solid Earth*, *118*(5), 2085–2101. https://doi.org/10.1002/jgrb.50139

Rioux, M., Garber, J., Bauer, A., Bowring, S., Searle, M. P., Kelemen, P. B., & Hacker, B. (2016). Synchronous formation of the metamorphic sole and igneous crust of the Semail ophiolite: New constraints on the tectonic evolution during ophiolite formation from high-precision U–Pb zircon geochronology. In *Earth and Planetary Science Letters* (Vol. 451). https://doi.org/10.1016/j.epsl.2016.06.051

Schwarzenbach, E. M., Früh-Green, G. L., Bernasconi, S. M., Alt, J. C., & Plas, A. (2013). Serpentinization and carbon sequestration: A study of two ancient peridotite-hosted hydrothermal systems. *Chemical Geology*, *351*, 115–133. https://doi.org/10.1016/j.chemgeo.2013.05.016

Schwarzenbach, E. M., Gill, B. C., Gazel, E., & Madrigal, P. (2016). Sulfur and carbon geochemistry of the Santa Elena peridotites: Comparing oceanic and continental processes during peridotite alteration. *Lithos*. https://doi.org/10.1016/j.lithos.2016.02.017

Searle, M. P., & Malpas, J. (1980). Structure and metamorphism of rocks beneath the Semail ophiolite of Oman and their significance in ophiolite obduction. *Transactions of the Royal Society of Edinburgh: Earth Sciences*, *71*(4), 247–262. https://doi.org/10.1017/S0263593300013614

Searle, M. P., & Malpas, J. (1982). Petrochemistry and origin of sub-ophiolitic metamorphic and related rocks in the Oman Mountains. *Journal of the Geological Society*, *139*(3), 235–248. https://doi.org/10.1144/gsjgs.139.3.0235

Searle, M. P., Waters, D. J., Martin, H. N., & Rex, D. C. (1994). Structure and metamorphism of blueschist-eclogite facies rocks from the northeastern Oman Mountains. *Journal - Geological Society (London)*, *151*(3), 555–576. https://doi.org/10.1144/gsjgs.151.3.0555

Searle, Michael P., & Cox, J. (2002). Subduction zone metamorphism during formation and emplacement of the Semail ophiolite in the Oman Mountains. *Geological Magazine*, *139*(3), 241–255. https://doi.org/10.1017/S0016756802006532

Soret, M., Agard, P., Dubacq, B., Plunder, A., & Yamato, P. (2017). Petrological evidence for stepwise accretion of metamorphic soles during subduction infancy (Semail ophiolite, Oman and UAE). *Journal of Metamorphic Geology*, *35*(9), 1051–1080. https://doi.org/10.1111/jmg.12267

Stanger, G. (1985). Silicified serpentinite in the Semail nappe of Oman. *Lithos*, *18*, 13–22. https://doi.org/10.1016/0024-4937(85)90003-9

Stewart, E. M., & Ague, J. J. (2020). Pervasive subduction zone devolatilization recycles CO2 into the forearc. *Nature Communications*, *11*(1), 1–8. https://doi.org/10.1038/s41467-020-19993-2

Tibi, R., Wiens, D. A., & Yuan, X. (2008). Seismic evidence for widespread serpentinized forearc mantle along the Mariana convergence margin. *Geophysical Research Letters*, *35*(13), 267–270. https://doi.org/10.1029/2008GL034163

Tsuji, Y., Nakajima, J., & Hasegawa, A. (2008). Tomographic evidence for hydrated oceanic crust of the Pacific slab beneath northeastern Japan: Implications for water transportation in subduction zones. *Geophysical Research Letters*, *35*(14), 1–5. https://doi.org/10.1029/2008GL034461

Weis, D., Kieffer, B., Maerschalk, C., Barling, J., De Jong, J., Williams, G. A., Hanano, D., Pretorius, W., Mattielli, N., Scoates, J. S., Goolaerts, A., Friedman, R. M., & Mahoney, J. B. (2006). High-precision isotopic characterization of USGS reference materials by TIMS and MC-ICP-MS. *Geochemistry, Geophysics, Geosystems*, *7*(8). https://doi.org/10.1029/2006GC001283

Weyhenmeyer, C. E. (2000). *Origin and evolution of groundwater in the alluvial aquifer of the Eastern Batinah Coastal Plain, Sultanate of Oman : a hydrogeochemical approach*. PhD Thesis, Universität Bern.

Wilde, A., Simpson, L., & Hanna, S. (2002). Preliminary study of tertiary hydrothermal alteration and platinum deposition in the Oman ophiolite. *Journal of the Virtual Explorer*, *6*, 7–13.

Yoshikawa, M., Python, M., Tamura, A., Arai, S., Takazawa, E., Shibata, T., Ueda, A., & Sato, T. (2015). Melt extraction and metasomatism recorded in basal peridotites above the metamorphic sole of the northern Fizh massif, Oman ophiolite. *Tectonophysics*, *650*, 53–64. https://doi.org/10.1016/j.tecto.2014.12.004